Synthesis, Structural Features, Absorption Spectra, Redox Behaviour and Luminescence Properties of Ruthenium(II) Rack-Type Dinuclear Complexes with Ditopic, Hydrazone-Based Ligands

Adrian-Mihail Stadler,[a] Fausto Puntoriero,[b] Sebastiano Campagna,*[b] Nathalie Kyritsakas,[c] Richard Welter,[d] and Jean-Marie Lehn*[a]

Abstract: The isomeric bis(tridentate) hydrazone ligand strands **1a–c** react with [Ru(terpy)Cl_3] (terpy = 2,2′:6′,2″-terpyridine) to give dinuclear rack-type compounds **2a–c**, which were characterised by several techniques, including X-ray crystallography and NMR methods. The absorption spectra, redox behaviour and luminescence properties (both in fluid solution at room temperature and in rigid matrix at 77 K) of the ligand strands **1a–c** and of the metal complexes **2a–c** have been studied. Compounds **1a–c** exhibit absorption spectra dominated by intense π–π* bands, which, in the case of **1b** and **1c**, extend within the visible region, while the absorption spectra of the rack-type complexes **2a–c** show intense bands both the in the UV region, due to spin-allowed ligand-centred (LC) transitions, and in the visible, due to spin-allowed metal-to-ligand charge-transfer (MLCT) transitions. The energy position of these bands strongly depends on the ligand strand: in the case of **2a**, the lowest energy MLCT band is around 470 nm, while in **2b** and **2c**, it lies beyond 600 nm. Ligands **1a–c** undergo oxidation processes that involve orbitals based mainly on the CH_3–N–N= fragments. The complexes **2a–c** undergo reversible metal-centred oxidation, while reductions involve the hydrazone-based ligands: in **2b** and **2c**, the bridging ligand is reduced twice and in **2a** once before reduction of the peripheral terpy ligands takes place. Ligands **1a–c** exhibit luminescence from the lowest-lying ^{1}π–π* level. Only for complex **2a** does emission occur; this may be attributed to a ^{3}MLCT state involving the bridging ligand. Taken together, the results clearly indicate that the structural variations introduced translate into interesting differences in the spectroscopic, luminescence and redox properties of the ligand strands as well as of the rack-type metal complexes.

Keywords: luminescence · N ligands · redox chemistry · ruthenium · supramolecular chemistry

[a] A.-M. Stadler, Prof. Dr. J.-M. Lehn
Laboratoire de Chimie Supramoléculaire, ISIS
Université Louis Pasteur, 8 Allée Gaspard Monge
BP 70028, 67083 Strasbourg Cedex (France)
Fax: (+33) 390-245-140
E-mail: lehn@isis.u-strasbg.fr

[b] Dr. F. Puntoriero, Prof. Dr. S. Campagna
Dipartimento di Chimica Inorganica
Chimica Analitica e Chimica Fisica, Università di Messina
Villaggio S. Agata, 96166 Messina (Italy)
Fax: (+39) 90-393756
E-mail: photochem@chem.unime.it

[c] N. Kyritsakas
Service Commun de Rayons X, Institut Le Bel
Université Louis Pasteur, 4 Rue Blaise Pascal
67000 Strasbourg (France)

[d] Prof. Dr. R. Welter
Laboratoire de Densité Electronique et Composés Métalliques
Institut Le Bel, Université Louis Pasteur
4 Rue Blaise Pascal, 67000 Strasbourg (France)

Introduction

Coordinative polynuclear heteroleptic complexes of ruthenium(II) with 2,2′:6′,2″-terpyridine (terpy) and polytopic heterocyclic ligand strands are the focus of interest for both their photophysical and electrochemical properties,[1,2] and as precursors for topological stereoisomers.[3] Such reasons have indeed stimulated large efforts to synthesize appropriate bis(tridentate) ligands[4] that are able to generate such metallosupramolecular architectures.[5]

In our laboratories, we are interested in developing facile synthetic pathways for analogues of helical ligands py_1-(py_2-pym)$_n$-py_2-py_1 (py_1 = 2-substituted pyridine, py_2 = 2,6-disubstituted pyridine, pym = 4,6-disubstituted pyrimidine), by replacing the 2,6-disubstituted pyridine ring by its isomorphic equivalent, a hydrazone (hyz) group.[6,7] This synthetic strategy has also the advantage of increasing the molecular di-

 DOI: 10.1002/chem.200401261

versity. For a ligand strand with two tridentate terpy-like sites (py_1-py_2-pym-py_2-py_1), replacing py_2 by a hydrazone group generates two types of two-site symmetric isomeric ligands, because the central unit may be derived from a bis-(hydrazino)pyrimidine or from a pyrimidine-dicarboxaldehyde. This isomerism means the change of the position of the C=N bond. Thus, one gains synthetic efficiency and simplicity, but also access to diverse molecular species, that is, to two possibilities for py_1-hyz-pym-hyz-py_1 (**1a** and **1b**), instead of one for py_1-py_2-pym-py_2-py_1 (Scheme 1). The same synthetic strategy may be applied for other two-site ligands, such as the py_1-py_2-pz-py_2-py_1 (pz = 2,5-disubstituted pyrazine) sequence,[8] the hydrazone analogue of which (**1c**) we report herein.

The ligands **1a–c** react with [Ru(terpy)Cl_3] in protic solvents, by heating to reflux, and give the corresponding dinuclear ruthenium(II) rack-type complexes, thus showing a remarkable stability of the C=N bond from the hydrazone groups. It could be expected that the spectroscopic, photophysical and electrochemical properties of the isomeric complexes (derived from these isomeric ligands) be different, due to changes of the C=N bond positions. Here we report the synthesis of the three ligands (**1a–c**) of such a class of molecule and of the three corresponding dinuclear rack-type ruthenium(II) complexes (**2a–c**) derived from these species. All the compounds have been characterized by several techniques, including various NMR methods and mass spectrometry. The rack-type complexes have also been investigated by X-ray analysis. Absorption spectra, redox behaviour and luminescence properties of the new metal complexes, as well as of the free ligands, have been studied. The results indicate that the molecular diversity introduced by the isomerism translates into interesting differences as far as the spectroscopic, luminescence and redox properties of the new compounds are concerned.

Abstract in French: *La réaction des ligands bidentates isomères de type bishydrazone **1a–c** avec [Ru(terpy)Cl_3], conduit aux complexes dinucléaires **2a–c**. Les études radiocristallographiques par diffractionole rayons X montrent que les complexes **2a,b** contenant le noyau pyrimidine 4,6-disubstitué comme unité centrale présentent une courbure, alors que le complexe **2c**, qui a pour unité centrale la pyrazine 2,5-disubstituée, est à peu près linéaire. Quand l'unité centrale est dérivée d'un dialdéhyde, les complexes sont verts (**2b,c**; absorption à 600 nm), alors que lorsqu'elle est dérivée d'une bishydrazine, le complexe correspondant **2a** est brun-rouge (absorption à 470 nm). Ce dernier est le seul complexe à présenter une émission, alors que les ligands **1a–c** sont tous luminescents. D'un point de vue électrochimique, les ligands **1a–c** participent à des processus irréversibles d'oxydation. Les complexes **2a–c** subissent des oxydations réversibles ou quasi-réversibles et présentent plusieurs réductions réversibles dans le domaine de potentiel de −2.00 à +2.00 V/ECS. Ces résultats mettent en lumière les modifications des propriétés structurales et physico-chimiques produites dans les complexes métalliques par le remplacement d'un noyau pyrimidine (**2a,b**) par un noyau pyrazine (**2c**) ou par le changement de position de la fonction hydrazone (**2a** et **2b,c**). Ils permettent d'envisager la synthèse de complexes de plus grande taille à sites multiples, présentant une courbure/linéarité et des propriétés contrôlables par la nature du ligand.*

Results and Discussion

Ligands synthesis: Ligands **1a–c** were synthesized (Scheme 2) by a double chain-extension method consisting of the condensation of 4,6-bis(1-methylhydrazino)-pyrimidine with 2-pyridinecarboxaldehyde (in case of ligand **1a**[7]) or of a dialdehyde (**4** or **5** with 2-(1-methylhydrazino)-pyridine (in case of ligands **1c**[7] and **1b**, respectively). Strands **1a** and **1b** have a C_2 symmetry axis, while strand **1c** has an inversion centre as a symmetry element.

Reaction of 2,5-dimethylpyrazine with benzaldehyde, in presence of benzoic anhydride, gave 2,5-distyrylpyrazine[9] (**6**), the ozonolysis (O_3, MeOH, −78 °C) of which, followed by reduction with aqueous solution of sodium metabisulfite ($Na_2S_2O_5$), produced 2,5-pyrazinedicarboxaldehyde[10] (**4**). Condensation of dialdehyde **4** with 2-(1-methylhydrazino)-pyridine[11] (**3**) in EtOH, at reflux, gave the ligand **1c**.

In ligands **1a–c**, the hydrazone group is the isomorphic equivalent[6,7] of a 2,6-disubstituted pyridine ring, so these ligands may be considered as analogues of ditopic ligands with two tridentate terpy-like sites. They have coordinative capacity to form heteroleptic ruthenium(II) rack-type complexes, playing the same role as the two-site ligand composed of py–pym[1a–d] or py–pz[8] sequences.

Complex synthesis: Rack-type complexes of ruthenium(II) may be formed by octahedral coordination of a Ru^{II} cation with three nitrogen atoms of a terpy ligand and three of a hydrazone site, so that a dihydrazone ligand could generate a dinuclear complex.

The complexes were prepared by following a pathway that has been described for the synthesis of racks containing py–pym ligands[1a–d] (Scheme 2). [Ru(terpy)Cl_3][12] was treated with ligands **1a–c**, in molar ratio 2.2:1, at reflux, in a mixture of protic solvents that have reducing properties (donors of electrons for the process $Ru^{III} + e^- \rightarrow Ru^{II}$). The used mixture was composed of 1:1 v/v water and an alcohol (ethanol or isopropanol), in which the reactants were heated at reflux during 18–21 h. The results showed that the hydrazone bonds were stable under these conditions, as complexation was achieved with yields comparable to those of the reactions involving the py–pym based ligands.[1a,d]

The obtained complexes have Cl^- as a counterion and are water soluble. They were precipitated from water by addition of PF_6^- as aqueous solution of ammonium hexafluorophosphate (NH_4PF_6). Further purification was performed by recrystallization from water and/or reprecipitation from CH_3CN with Et_2O or chloroform.

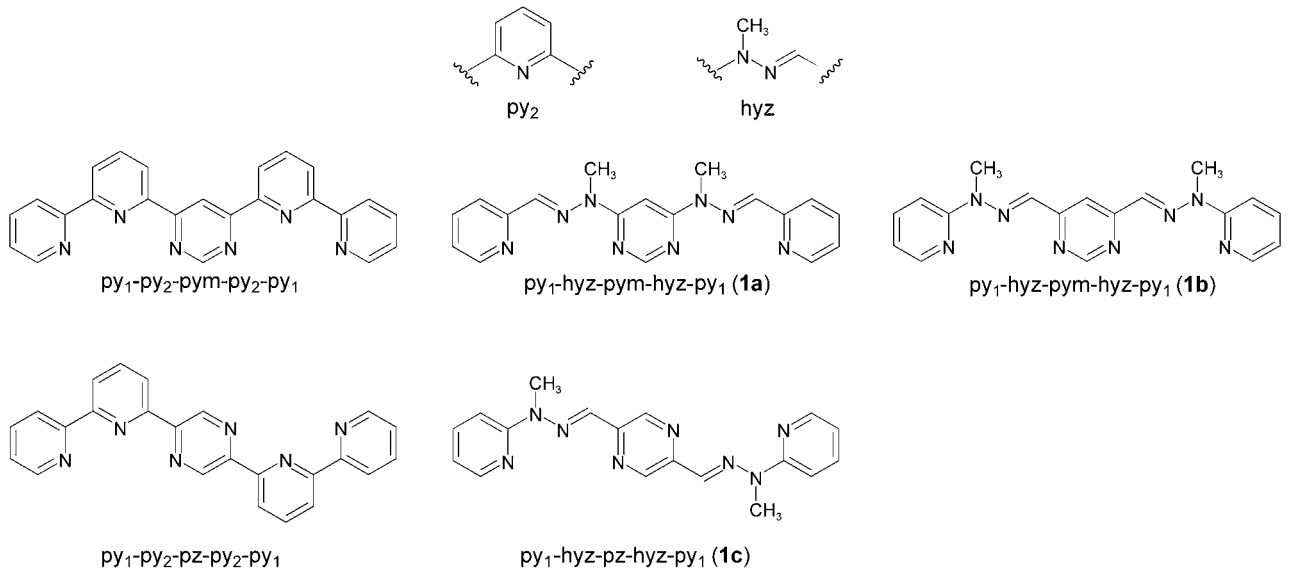

Scheme 1. The replacement of a 2,6-disubstituted pyridine (py_2) by a hydrazone (hyz) group provides efficient access to analogue isomeric strands with similar coordinative properties.

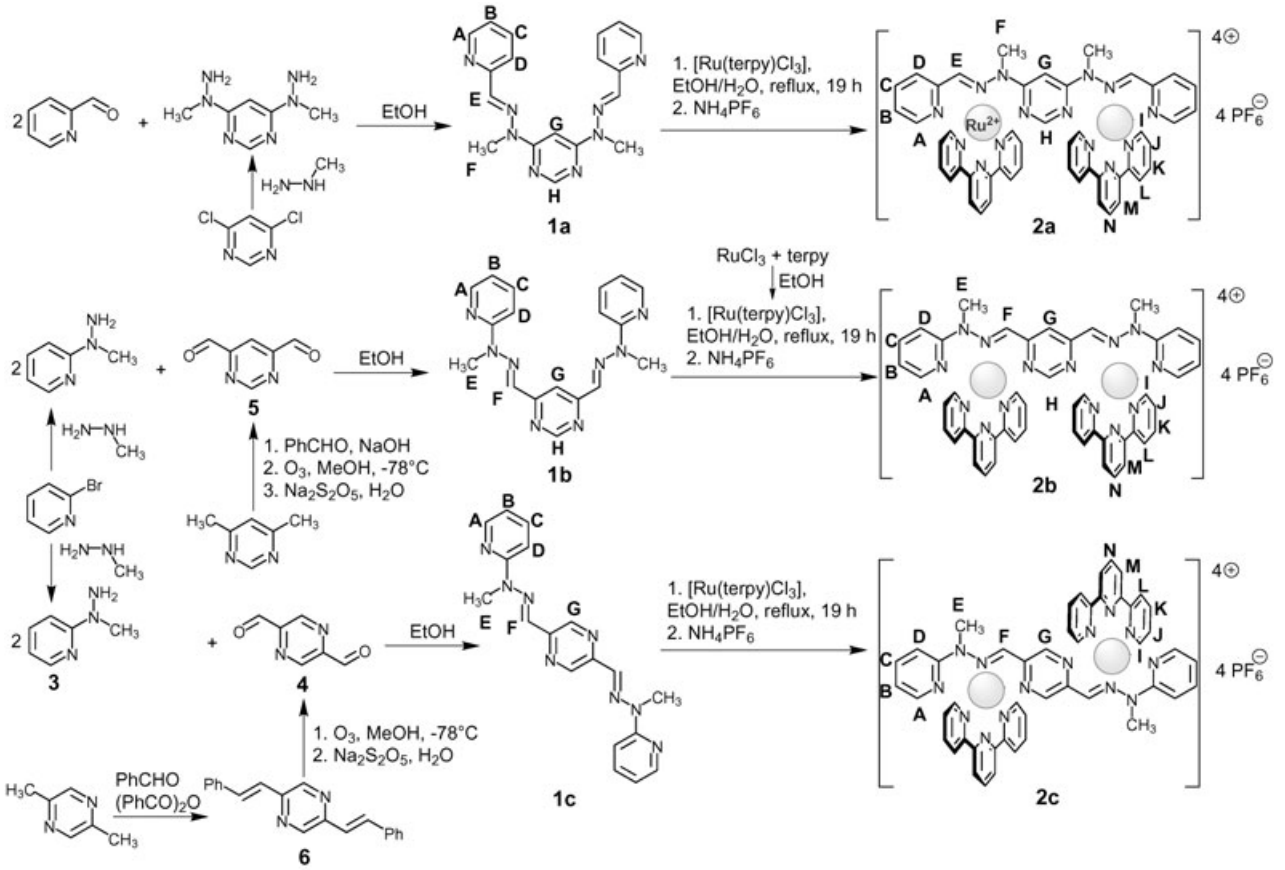

Scheme 2. Synthesis of the ligands **1a**–**c** and of the complexes **2a**–**c**. The notations for the protons are also indicated.

The complexes are coloured, solid materials (**2a** is brown-red, **2b** and **2c** are deep green), soluble in acetonitrile, acetone and nitromethane, but insoluble in toluene, diethyl ether, diisopropyl ether, benzene and chloroform, a fact that was used in crystallization experiments to obtain single crystals. On heating, they decompose at temperatures greater than 300 °C.

Crystallographic studies: Single crystals suitable for X-ray diffraction were obtained by slow diffusion of Et_2O into a solution of complexes **2a** or **2b** in CH_3CN/CH_3OH (9:1) and of iPr_2O in a solution of complex **2c** in CH_3CN. Crystals of **2a** are triclinic, crystals of **2b** are monoclinic and those of **2c** are triclinic. Complex **2a** crystallizes as a dimer with four molecules of acetonitrile, one molecule of methanol and two molecules of water ($2\,C_{48}H_{40}N_{14}Ru_2P_4F_{24}\cdot 4\,CH_3CN\cdot CH_3OH\cdot 2\,H_2O$), the crystal cell containing two such units. Complex **2b** cocrystallizes with three molecules of acetonitrile ($C_{48}H_{40}N_{14}Ru_2P_4F_{24}\cdot 3\,CH_3CN$) and the crystal cell contains four such units. Complex **2c** has an inversion centre and cocrystallizes with six molecules of acetonitrile, the crystallographic unit is ($C_{48}H_{40}N_{14}Ru_2\cdot 4\,PF_6\cdot 6\,CH_3CN$)/2 and the crystal cell contains two such units.

All the measured distances are internuclear (centroid-to-centroid) distances. The Ru–Ru distance is 6.14 Å for **2a** (average distance), 6.13 Å for **2b** and 6.89 Å for **2c**. For the pyrimidine-based ligands, the coordinated two-site ligand strand is not perfectly linear but curved, and its length is 17.66 Å for **2a** (average values: calculated curve radius $r=12.61$ Å; curvature $\kappa=1/r=7.93\cdot10^{-2}$ Å^{-1}; arc central angle: 89°) and 17.64 Å for **2b** (calculated curve radius $r=12.84$ Å; curvature $\kappa=7.79\cdot10^{-2}$ Å^{-1}; arc central angle: 86.5°), which shows that the hydrazone two-site ligands have almost identical dimensions in these two racks (Figure 1a). These two ruthenium(II) racks are shorter and more curved than the corresponding lead(II) racks (average length 18.20 Å[13]). This results from pinching at the coordinated centres due to the shorter binding distances of Ru^{II} in comparison with lead(II). Such pinching, resulting in curved structures, has been documented in related complexes.[1b] With the pyrazine-based ligand, the complex (**2c**) is globally linear (Figure 1a) due to the compensation of the coordinative contraction of the two py_1-hyz-pz tridentate sites thanks to the inversion centre; its length is 17.31 Å (here also less than the corresponding lead(II) complex, 18.10 Å[13]).

In both **2a** and **2b**, the two terpy ligands are crystallographically unequivalent and the observation of identical NMR signals are due to fast NMR timescale motions in solution, which make these terpy units equivalent. In complex **2c**, the two terpy moieties are equivalent. The length of coordinated terpy is 11.15 Å. In **2a** and **2b**, the planes of terpy ligands are not parallel and make an angle of about 32° (31.4° for **2a**, average value, and 32.9° for **2b**) in the longitudinal section that contains the plane of the two-site ligand, neither are they perpendicular to the plane of the two-site ligand. In contrast in complex **2c**, the terpy planes are parallel and almost perpendicular to the plane of pyrazine-based ligand. For the pyrimidine derivatives, the shortest distance between the terpy planes is about 3 Å (3.08 Å for **2a**, average value, and 2.95 Å for **2b**), but the other distances (mainly larger than 4 Å), as well as the nonparallel orientation of the two molecular planes in **2a** and **2b**, suggest that there is no π-stacking between the aromatic rings of these two molecules. In **2c**, the distance between terpy planes is 6.70 Å and the distance between the K protons of two different terpy moieties is 8.22 Å (Figure 1a). The cavity generated by the two terpy ligands is empty in the case of **2b**. In the case of **2a**, one unit of the dimer has a water molecule between two of the terminal pyridine rings of this cavity, whereas in the other unit the cavity is empty.

The analysis of the pseudo-octahedral coordinative environment of the ruthenium(II) ions from the X-ray structures of complexes **2a–c** provided the Ru–N bond lengths compiled in Table 1 (for the notations see also Figure 1b; for complex **2a** crystallized as a dimer, the numbering of Ru and N coordinating atoms is shown on a monomer; for both complexes **2a** and **2b**, the numbering of Ru atoms is the same as in the corresponding crystallographic information files (CIF)). The average Ru–N length in the complexes is 2.038 Å. In the tridentate sites the distance between the Ru atom and the middle N atom is shorter (average value 1.980 Å) than the two other Ru–N distances (average value 2.067 Å). The average distance between the middle N_{hyz} atom and Ru (1.974 Å) is comparable with the corresponding one from the terpy site (1.986 Å), thus confirming the analogous coordinative properties of the two N atoms.

The average value of the N-Ru-N chelating angles is 78.9°, that is, 10.1° less than the ideal angle for an octahedral coordination (90°). The values corresponding to each chelating angle are listed in Table 2.

NMR spectroscopy: The ^{1}H NMR spectra of **1a–c** are given in Figure 2. The pyridine protons (marked A–D) and the methyl group (E) from the ligand **1c** give rise to signals that are similar to the corresponding protons of ligand **1b**; this is because the terminal pyridine units in both ligands **1b** and **1c** are identical. The two protons of the pyrazine ring are equivalent, while the protons of pyrimidine ring are not. Although the pyrazine proton (G) it is not located on a carbon atom situated between two N atoms, as the C2 proton from the pyrimidine ring (proton H) is, its chemical shift has a value (9.16 ppm) close to that of the pyrimidine C2 proton (9.08 ppm). This could be explained by the strong deshielding effect due to the proximity to an N atom and to the two *para*-conjugated –C=N– groups located on the pyrazine ring.

The ^{1}H NMR spectra of complexes **2a–c** are relatively complicated (Figure 2), due to close signals in the aromatic region, and two-dimensional experiments (COSY, NOESY, ROESY) were useful for the peak assignment. Some particularities should be noted.

All the complexes, as well as the two-site ligands, are "lateral" and "alternate" structural isomers. Complexes **2a**,**b** have C_2 symmetry, and 14 groups of NMR-equivalent protons; the complex **2c** has an inversion centre (from the ligand **1c**) and it displays only 13 groups of NMR-equivalent protons.

The presence of the two terpy ligands (with the magnetic anisotropy of the aromatic rings), as well as the metal-ion coordination induce shielding ($\delta_{complex}-\delta_{free\ ligand}=\Delta\delta<0$) or deshielding ($\Delta\delta>0$) effects. Thus, for complexes **2a** and **2b**, the zone between the two terpy moieties should be the most

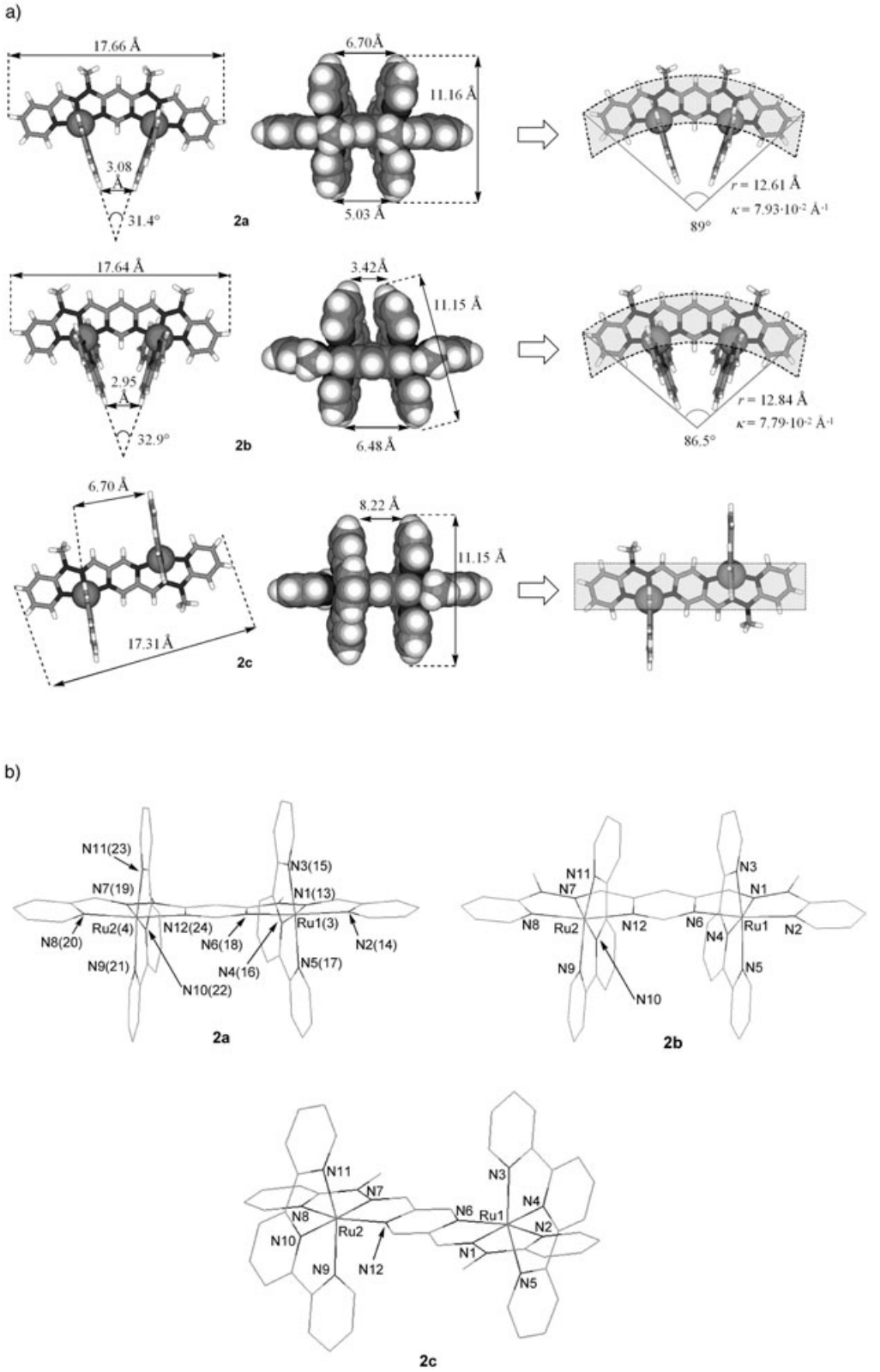

Figure 1. a) Representation of the X-ray molecular structures of complexes **2a**, **2b** and **2c** (PF_6^- ions and solvent molecules are omitted for clarity); r is the curve radius and κ is the curvature ($\kappa = 1/r$). b) Notations for coordinating N atoms and Ru atoms in complexes **2a–c**.

shielded from the molecule, a fact confirmed by the extremely low chemical shift of the C2 pyrimidine proton (proton H; see Figure 2 and Table 3). On the other hand, in the complex **2c**, due to the inversion centre of the ligand **1c**,

Table 1. Ru–N bond lengths [internuclear distances, Å] from the X-ray structures of complexes **2a–c**[a].

	Ru1–N1 Ru2–N7 Ru3–N13[b] Ru4–N19[b]	Ru1–N2 Ru2–N8 Ru3–N14[b] Ru4–N20[b]	Ru1–N3 Ru2–N11 Ru3–N15[b] Ru4–N23[b]	Ru1–N4 Ru2–N10 Ru3–N16[b] Ru4–N22[b]	Ru1–N5 Ru2–N9 Ru3–N17[b] Ru4–N21[b]	Ru1–N6 Ru2–N12 Ru3–N18[b] Ru4–N24[b]
2a	1.976(6)	2.069(6)	2.070(7)	1.976(6)	2.058(7)	2.066(6)
	1.975(6)	2.057(7)	2.062(7)	1.974(7)	2.057(7)	2.064(6)
	1.978(6)	2.079(6)	2.056(7)	1.990(7)	2.066(8)	2.056(6)
	1.976(7)	2.069(7)	2.082(7)	1.986(7)	2.062(7)	2.072(7)
2b	1.963(4)	2.060(4)	2.081(5)	1.989(4)	2.059(5)	2.052(4)
	1.965(4)	2.070(4)	2.067(4)	1.981(4)	2.074(4)	2.049(4)
2c	1.977(3)	2.071(4)	2.080(3)	1.995(3)	2.084(3)	2.060(3)
	1.977(3)	2.071(4)	2.084(3)	1.995(3)	2.080(3)	2.060(3)

[a] Notations: hydrazone C=N nitrogen atoms (N_{hyz}): N1, N7, N13, N19; pyrimidine nitrogen atoms: N6, N12, N18, N24; terpy nitrogen atoms: N3, N4, N5, N9, N10, N11, N15, N16, N17, N21, N22, N23; pyridine nitrogen atoms from the two-site ligand: N2, N8, N14, N20. [b] Only for **2a**.

Table 2. Values of N-Ru-N chelating angles [°] from the X-ray structures of complexes **2a–c**[a].

	N1-Ru1-N2 N7-Ru2-N8 N13-Ru3-N14[b] N19-Ru4-N20[b]	N1-Ru1-N6 N7-Ru2-N12 N13-Ru3-N18[b] N19-Ru4-N24[b]	N3-Ru1-N4 N10-Ru2-N11 N15-Ru3-N16[b] N22-Ru4-N23[b]	N4-Ru1-N5 N9-Ru2-N10 N16-Ru3-N17[b] N21-Ru4-N22[b]
2a	79.1(3)	78.9(3)	79.4(3)	79.2(3)
	79.3(3)	78.4(3)	79.5(3)	79.1(3)
	78.8(3)	78.5(3)	78.7(3)	78.5(3)
	79.3(3)	78.7(3)	78.4(3)	79.4(3)
2b	79.5(2)	79.3(2)	79.4(2)	79.1(2)
	78.7(2)	79.1(2)	79.1(2)	78.9(2)
2c	78.5(1)	79.1(1)	78.3(1)	78.5(1)
	78.5(1)	79.1(1)	78.5(1)	78.3(1)

[a] For the notations, see Figure 1b. [b] Only for **2a**.

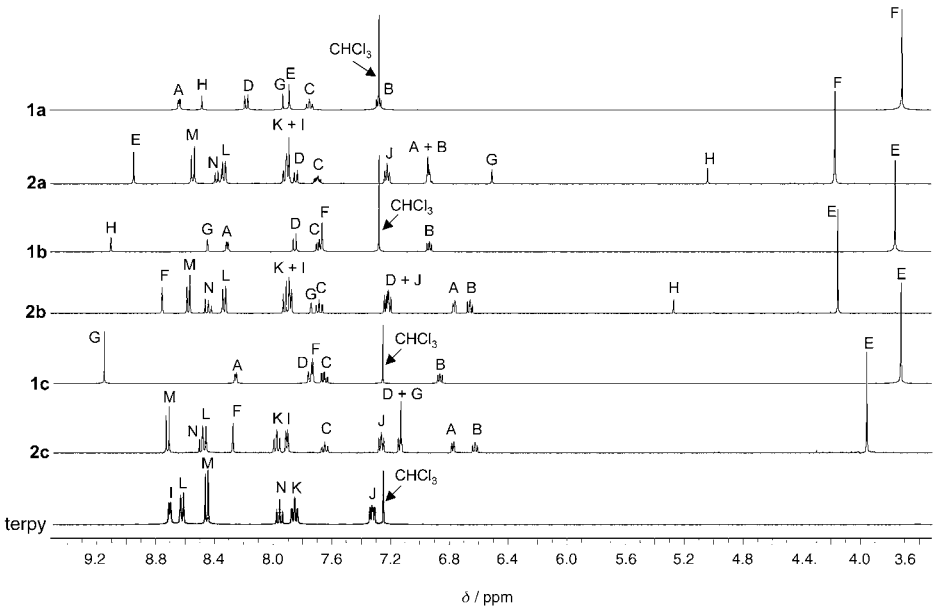

Figure 2. ^{1}H NMR (400 MHz) spectra and peak assignment for ligands **1a–c** (solvent $CDCl_3$), complexes **2a-c** (solvent CD_3CN) and terpy (solvent $CDCl_3$). For the notations of the protons, see Scheme 2.

the two terpy units are on opposite sides of the rack and this makes their shielding effect on proton G weaker than in the case of proton H from **2a** and **2b** (for the $\Delta\delta$ value, see Table 3).

The shielding of the C5 proton of the pyrimidine ring (proton G) is also an effect of the coordination process, already observed in the case of complexes of **1a** and **1b** with lead(II).[13] The chemical shift variation is important (for the $\Delta\delta$ values, see Table 3). This is due to the presence of the terpy units (as for the protons D), but also to a conformational change of the ligand by coordination. In the case of **1a**, the coordination causes rotation around the $C4_{pym}$–N bond and the place of the N–N bond is taken by the N–CH_3 bond, so that the deshielding C=N bond and the N lone pair close to proton G are replaced by a methyl group. In the case of **1b**, the coordination causes rotation around the $C4_{pym}$–$C_{=N}$ bond move and the place of the deshielding C=N bond and of the N lone pair is taken by the =C–H bond.

The coordination of ruthenium(II), as well as the localization of hydrazone group protons (CH_3 and $H_{C=N}$) in the deshielding zone of the two terminal pyridine rings of the terpys, make the chemical shift of the methyl and imine protons higher in the complexes than in the free ligands (for the $\Delta\delta$ values, see Table 3). The opposite orientation of tridentate sites in **2c** generates a proximity between the hydrazone group and the three rings of the other terpy ligand; this should induce a stronger shielding of the methyl group and of the proton of the hydrazone bound in **2c**, relative to that found in **2a** or **2b** (Figure 2 and Table 3).

With respect to the free two-site ligands, the resonances of

Table 3. Chemical shifts of the protons in free (**1a–c**) and complexed (in **2a–c**) two-site ligands.

	H_A	H_B	H_C	H_D	CH_3	$H_{hydrazone}$	H_G	H_H
1a δ_{ligand}[a]	8.61	7.25	7.73	8.15	3.70	7.87	7.91	8.47
2a $\delta_{complex}$[a]	6.92[c]	6.92[c]	7.68	7.82	4.15	8.93	6.49	5.02
$\Delta\delta$[b]	−1.69	−0.33	−0.05	−0.33	0.45	1.06	−1.42	−3.45
1b δ_{ligand}	8.29	6.92	7.66	7.83	3.74	7.64	8.42	9.08
2b $\delta_{complex}$	6.75	6.65	7.67	7.20[c]	4.14	8.74	7.73	5.26
$\Delta\delta$	−1.54	−0.27	0.01	−0.63	0.40	1.10	−0.69	−3.82
1c δ_{ligand}	8.26	6.87	7.66	7.60	3.73	7.74	9.16	–
2c $\delta_{complex}$	6.78	6.63[c]	7.65	7.14	3.96	8.28	7.15	–
$\Delta\delta$	−1.48	−0.24	−0.01	−0.46	0.23	0.54	−2.01	–

[a] In ppm. [b] $\Delta\delta = \delta_{complex} - \delta_{ligand}$. [c] Central position of the multiplet.

the protons of the terminal pyridines change in the complex. In the case of protons A, B and D, a shielding effect is observed. The most shielded pyridine proton is proton B. The most dramatic shift change due to the shielding is observed for proton A. The chemical shift of proton C is the less affected by the complex formation (Table 3).

The integration of terpy units into the complex by coordination causes a shielding of protons I, J and L, but a deshielding of protons K, M and N, relative to the free terpy moiety (see Table 4). The stronger shielding effect is observed for the proton I, the average shift decrease being of around 0.82 ppm. The stronger deshielding is noted for the proton N, the average increase of the chemical shift being 0.46 ppm. Proton K is, similarly to proton C, less affected by the coordination. The proximity of the two terpy groups also generates in the case of **2a** and **2b** a reciprocal shielding of their protons, whose chemical shifts are generally inferior to the corresponding ones of **2c**, while the shifts of terpy protons have almost identical values in **2a** and **2b** (Table 4).

Table 4. Chemical shifts of terpy protons in the free terpy ligand and in complexes **2a–c**.

		H_I	H_J	H_K	H_L	H_M	H_N
terpy	δ[a]	8.71	7.33	7.86	8.62	8.45	7.96
2a	δ	7.89	7.20	7.89	8.31	8.52	8.35
	$\Delta\delta$[b]	−0.82	−0.13	0.03	−0.31	0.07	0.39
2b	δ	7.87	7.20[c]	7.90	8.32	8.56	8.43
	$\Delta\delta$	−0.84	−0.13	0.04	−0.30	0.11	0.47
2c	δ	7.91	7.27	7.98	8.47[c]	8.72	8.49[c]
	$\Delta\delta$	−0.80	−0.06	0.12	−0.15	0.27	0.53

[a] In ppm. [b] $\Delta\delta = \delta_{complex} - \delta_{free\ terpy}$. [c] Central position of the multiplet.

The shape of the coordinated two-site strands as represented in the structural formula were confirmed by 2D NMR experiments, essentially by correlations due to the existence of NOEs (nuclear Overhauser effects) between several key-protons closely involved in the conformational change of the ligand before and after binding of the metal ion. The coordination induces the transformation of the all-*transoid* conformation into an all-*cisoid* one. In the case of terpy, it produces the (L,M) NOE correlations observed for all complexes **2a–c**. The shape of the 2-hydrazone-site coordinated ligand was established by NOE correlations that do not exist in the free ligand, but appear after coordination: (D, E) and (F, G); simultaneously, the (D, G) correlation characteristic to the free ligands **1a–c** disappeared (for the NOESY of complex **2c**, see Figure 3). Moreover, correlations corresponding to a NOE between the proton E from the hydrazone strand and the proton I of the terpy unit, but also between the protons F and I were observed; this confirms the space proximity between the two coordinated terpy units and the **1a–c** coordinated strands in the complex **2a–c**.

Redox behaviour: Cyclic and differential pulse voltammetries have been employed to investigate the redox behaviour of the new compounds. For solubility reasons, the free ligands were studied in 1,2-dichloroethane and the metal

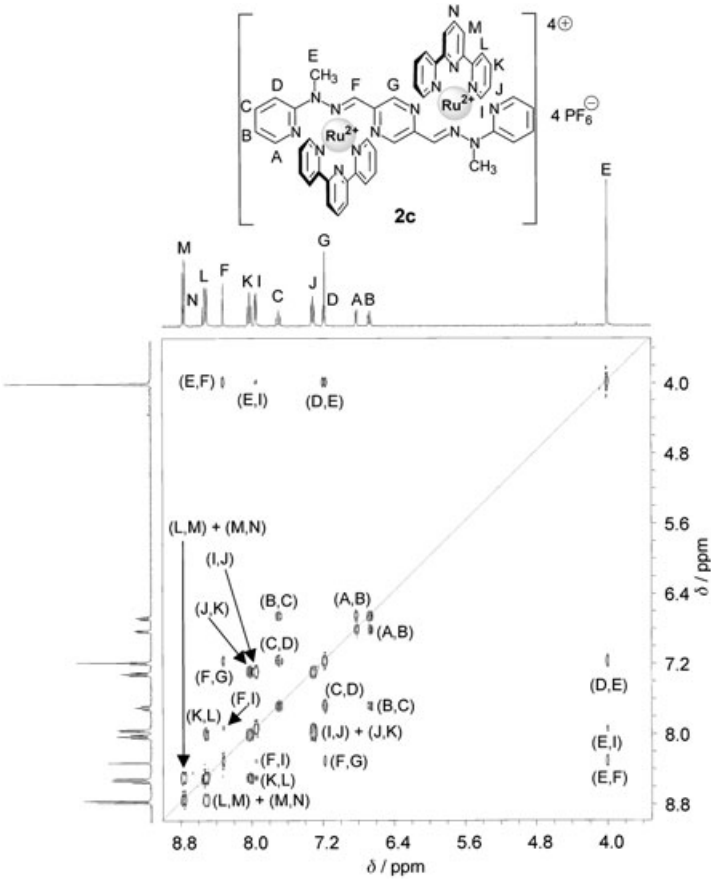

Figure 3. ^1H-^1H NOE correlations for the complex **2c** (NOESY experiment, 300 MHz, CD_3CN).

complexes in acetonitrile. Data are reported in Table 5. Detailed discussion of the various processes is as follows.

Free ligands: Compounds **1a–c** undergo two irreversible oxidation processes at relatively mild potentials and no reduction process takes place within the potential window investigated (−2.00/+2.00 V vs SCE). As far as the first oxidation process of **1a–c** is concerned, while for **1a** and **1b** it take place at similar potentials, that of **1c** occurs at a significantly less negative potential (Table 5). This suggests that the central pyrazine ring has an important role in determining the oxidation potential of **1c**. Such a role can be interpreted in a simple way as follows: in all the cases the orbital involved in the oxidation process (i.e., the HOMO of the molecule) should receive large contributions from a CH_3–N–N= framework (probably with the largest contribution involving the nitrogen atom carrying the methyl group), and the other moieties can be seen as substituents of the redox-active unit. Pyrimidine is a better electron-withdrawing group than pyrazine, so the orbitals of the redox-active unit of **1c** are less stabilized than those of **1a** and **1b** by the central ring. As a consequence, **1c** is oxidized more easily. Such a line of reasoning could also explain the difference between the oxidation potentials of **1a** and **1b** (Table 5), since the redox-active orbital would be closer to the electron-withdrawing pyrimidine ring (and therefore more affected electronically and stabilized) in **1a**. The second oxidation process exhibited by all the three ligand strands is easily interpreted by considering that each ligand has *two* CH_3–N–N= frameworks, so first oxidation is mainly centred on one of these sites and the second on the remaining one. This assignment agrees with the potential separation between the two oxidation processes in the ligand strands, which is related to the electronic interactions between the hydrazone-based moieties and decreases in the series **1a**, **1b**, **1c** (Table 5). The distance between the redox active sites (inversely proportional to the electronic interactions) within each ligand indeed decreases with the same trend.

Table 5. Absorption, luminescence, and redox data.

	Absorption[a]	Luminescence[b]		Redox Data[c]	
	298 K, λ_{max} [nm] (ε [$M^{-1}cm^{-1}$])	298 K,[a] λ_{max} [nm] (τ [ns])	77 K,[d] λ_{max} [nm] (τ [ns])	$E_{1/2}$ (ox) [V vs SCE]	$E_{1/2}$ (red) [V vs SCE]
1a	284 (26800)	395 (16)	390 (630)	+1.30[e]	
	314 (43200)			+1.50[e]	
	340 (36500)				
1b	242 (27600)	432 (8)	469 (560)	+1.23[e]	
	335 (45150)			+1.33[e]	
	379 (32200)				
1c	247 (30200)	468 (10)	449 (542)	+1.04[e]	
	409 (67700)			+1.10[e]	
2a	226 (58900)	758 (30)	741 (335)	+1.28	−0.98
	270 (47000)			+1.53	−1.22
	308 (70300)			+1.78	−1.35[f]
	330 (60300)				
	362 (52200)				
	434 (22400)				
	470 (20700)				
2b	240 (42500)			+1.36	−0.45
	270 (48000)			+1.66	−1.05
	304 (61100)				−1.46
	330 (42500)				−1.65[f]
	430 (45700)				
	506 (12600)				
	630 (27000)				
2c	272 (56700)			+1.27	−0.50
	280 (53300)			+1.50	−1.05
	304 (72300)				−1.49
	440 (47400)				−1.57[f]
	614 (40600)				
	772 (2700)				

[a] For **1a–c**, data are in argon-purged dichloromethane; for **2a–c** in argon-purged acetonitrile. [b] Luminescence quantum yields at room temperature are not reported, since in all the cases they were lower than 10^{-4}, and accurate determination was difficult. [c] For **1a–c** the measurements were performed in argon-purged 1,2-dichloroethane, for **2a–c** in argon-purged acetonitrile. [d] In MeOH/EtOH 4:1 (v/v) matrix. [e] Irreversible process. [f] Other irreversible processes take place at more negative potentials, but they are not discussed here.

Rack-type metal complexes: All the rack-type complexes **2a–c** undergo two reversible or quasi-reversible oxidation processes and several reduction processes in the potential window examined (see Table 5 and Figure 4). The oxidation processes are easily assigned as being metal-centred. Actually, the oxidation potentials are close to those of other ruthenium(II) rack-type complexes,[1a–d] for which metal-centred oxidations have been reported. It has also to be considered that the ligand-based orbitals are expected to be significantly stabilized by coordination of the (positively charged) metal centres, so that their oxidations, which in the free ligands are quite close to the potentials of the oxidation of the metal racks, are here expected to occur to more positive potentials.[14]

Splitting of the oxidation processes in symmetric dinuclear metal complexes is due to 1) electronic interaction between the metal-based orbitals mediated by superexchange through the bridging ligand orbitals, which depends (beside other factors) on the energy separation between the full metal-based $d\pi$ and the empty

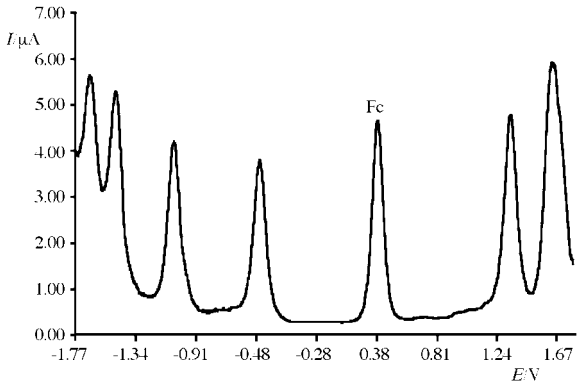

Figure 4. Differential pulse voltammogram of **2b** in acetonitrile solution. The peak at about 0.4 V is ferrocene, used as an internal standard. Working electrode: glassy carbon (8 mm^2, Amel) electrode. Counter electrode: a Pt wire. Reference electrode: SCE separated with a fine glass frit. The concentration of the complex was about 5×10^{-4} M. Tetrabutylammonium hexafluorophosphate (0.05 M) was used as supporting electrolyte. Scan rate: 20 $mV\,s^{-1}$.

bridging ligand-based π* orbitals, and 2) electrostatic interactions.[15] In spite of the first-sight similitude among **2a–c**, these species are different one another from an electronic viewpoint: complexes **2b** and **2c** differ from each other by the central ring of the bridge (pyrimidine vs. pyrazine); this also introduces differences in the distances between the metal centres (although relatively slight; compare the Ru–Ru distances reported in the crystallographic section, 6.13 vs. 6.89 Å for **2b** and **2c**, respectively). On the other hand, complex **2a** differs from the other two rack-type complexes because of the energy level and the much more localized nature of the bridging ligand-centred LUMO (see later the discussion of the reduction processes). It is hard to discuss in full detail the differences in the oxidation splitting among the complex series (250, 300 and 230 mV for **2a**, **2b** and **2c**, respectively), because they arise from various factors whose relative contributions are difficult to evaluate. As a matter of fact, the larger oxidation splitting of **2b** relative to **2c** is certainly due to the nature of the central ring of the bridge, while when compared to **2a** can be mainly attributed to the energy difference between the orbitals involved in the superexchange mechanism.

For the sake of convenience, we start the discussion of the reduction processes from **2b** and **2c**. Both these species show four one-electron reduction processes at very similar potentials. The first two processes take place at potentials less negative than the first terpy-based reduction occurring in $[Ru(terpy)_2]^{2+}$ (−1.25 V vs SCE),[14] so they are both attributed to the bridging ligands. In particular, reduction can be assigned to the central part of the bridging ligand strand, involving a delocalized orbital that receives dominant contributions from the pyrimidine/pyrazine ring and the two conjugate C=N double bonds. The difference in potential between the first two processes (600 and 550 mV for **2b** and **2c**, respectively) also agrees with the electron-pairing energy expected for such orbitals.[16] The third and fourth reduction processes of **2b** and **2c** are assigned to the first reduction of the two terpy ligands.

As far as the reduction behaviour of **2a** is concerned, the first reduction is still attributed, as for the other racks, to the first reduction of the bridging ligand; however, it occurs at a potential that is far more negative than that for first reduction of **2b** and **2c**. This is due to the nature of the orbital involved, which in **2a** is essentially localized on the bis-coordinated pyrimidine, with negligible contribution from the hydrazone moieties and missing extensive conjugation with the C=N double bonds. In contrast to the other racks, the second reduction of **2a** cannot be assigned to a second reduction of the same pyrimidine site: in fact, potential separation between first and second processes in **2a** is too small (240 mV) to be attributed to electron pairing. Therefore, both the second and third processes are assigned to the terpy units. Interestingly, the potential separation between the two terpy-centred processes is 130 mV (Table 5), smaller with respect to that found in the isomeric species **2b**, in spite of the structural similarity. Whereas a different interaction through the bridging ligand cannot be excluded, coulombic reasons could also play a role: as shown by X-ray determination (see above and also Figure 1a); the distance between coordinated terpy groups is smaller in **2b** than in **2a**.[17]

For all the complexes, further reduction processes take place at more negative potentials, but they are ill-defined and will not be discussed here.

Absorption spectra: The absorption spectra of the free ligands (solvent: dichloromethane) show moderately intense bands in the 260–460 nm spectral region (see Figure 5a and Table 5). For such ligands, both spin-allowed π–π* and n–π* transitions are expected,[18,19] with the latter having lower extinction coefficients. The absorption spectrum of terpy displays one band peaking at 280 nm, due to the spin-allowed π–π* transition, and a weak band around 340 nm, due to n–π* transitions.[14,19] The relatively high absorption coefficients of the bands which dominate the spectra of **1a–c** suggest that such bands are due to spin-allowed π–π* transitions. Figure 5a shows a progressive increase of the λ_{max} of the lowest energy band in the following order: **1a** (340 nm), **1b** (379 nm) and **1c** (409 nm). This bathocromic effect can be explained by the nature of the diazine rings and by the increase of conjugation between the heteroaromatic ring and the C=N bonds. On increasing the conjugation, the energetic difference between the π and π* levels decreases, so the wavelength of the corresponding π–π* transitions increases. In **1a**, the lowest energy bands receive contributions from π–π* transitions involving orbitals localized on the central pyrimidine ring or in the "peripheral" pyridine–hydrazone moieties. In **1b**, there are two chromophoric C=N bonds in conjugation with the same pyrimidine ring, in *meta* orientation. The lowest energy band is therefore here assigned to a π–π* transition delocalized over the central moiety of the ligand and is red-shifted relative to that of **1a**. When the orientation of the two C=N bonds is *para*, as in

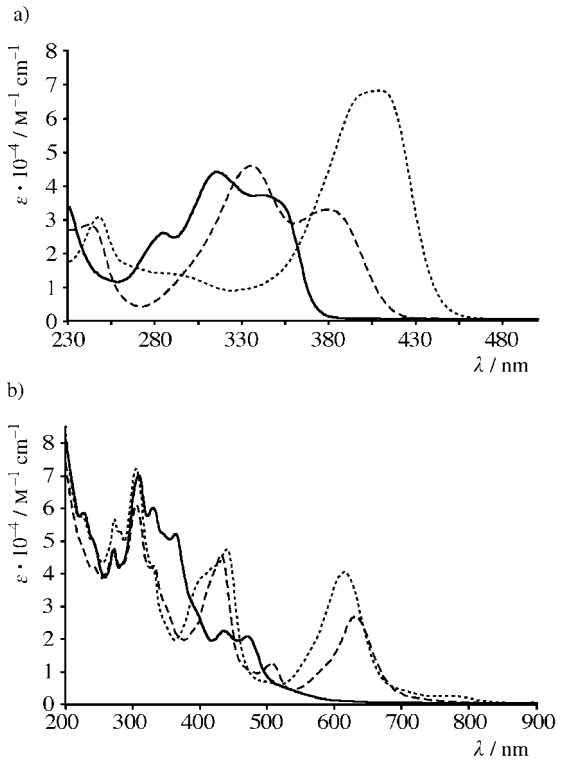

Figure 5. a) Absorption spectra of **1a** (solid line), **1b** (dashed line) and **1c** (dotted line) in dichloromethane. b) Absorption spectra of **2a** (solid line), **2b** (dashed line) and **2c** (dotted line) in acetonitrile.

1c, the conjugation is improved and the π–π* transition is at even lower energies. In all the ligands, the lower intensity n–π* bands are probably obscured, so their positions are not experimentally defined. It should be considered anyway that in hydrazone molecules containing electron-withdrawing groups (in the present case, diazine rings), the π–π* transitions can have some charge-transfer character,[20] also induced by mixing between π–π* and n–π* states. This can have important effects in particular as far as the deactivation processes are concerned (see luminescence section).

The absorption spectra of the rack-type metal complexes (Figure 5b, Table 5; solvent: acetonitrile) exhibit intense bands both in the UV and in the visible region. For all the complexes, the bands in the UV region receive main contributions from spin-allowed ligand-centred (LC) transitions (namely, π–π*) involving the terpy ligands (in particular, the band peaking at about 310 nm, common to all the species, is attributed to terpy-centered transitions), with the contribution from LC transitions involving the bridging ligands; this becomes especially relevant in the case of **2a**. The bands peaking at 430 and 440 nm in the spectra of **2b** and **2c**, respectively, are attributed to superposition of the lowest lying LC transitions involving the bridging ligands and the spin-allowed metal-to-ligand charge-transfer (MLCT) transitions involving terpy ligands. In **2a**, the lowest lying LC band occurs in the UV region, so that the absorption between 400 and 500 nm probably receives contributions only from MLCT transitions involving the terpy ligands. As far as the intense bands at $\lambda > 600$ nm of **2b** and **2c** are concerned, they can be attributed to spin-allowed MLCT transitions involving the −N=C−diazine−C=N− central moiety of the bridge as the acceptor orbital, while the corresponding Ru-to-bridge CT transition in **2a**, involving the much more difficult-to-reduce "isolated" pyrimidine fragment of the bridging ligand, is probably responsible for the broad absorption between 500 and 600 nm of **2a**.

Finally, the spectrum of **2c** also shows a relatively weak band at about 775 nm (Table 5, Figure 5b). We tentatively attribute such a weak band to a spin-forbidden singlet-triplet MLCT transition. Actually, ^{3}MLCT absorption bands are hardly discernable in ruthenium(II) complexes. Although never mentioned in mononuclear complexes, a few cases have been reported in multinuclear complexes. In particular, non-negligible spin-forbidden MLCT absorption has been mentioned in a tetranuclear species containing 2,3-bis(2′-pyridyl)pyrazine as a bridging ligand.[21] Interestingly, that bridging ligand and the one in **2c** share a pyrazine ring as the central subunit of the bridge. This could justify why the spin-forbidden transition is visible in **2c** but not in **2a** and **2b**.

Luminescence properties: The luminescence properties of the free ligands **1a–c** and of the rack-type complexes **2a–c** have been investigated in dichloromethane (free ligands) and acetonitrile (complexes) fluid solution at room temperature and in an MeOH/EtOH 4:1 (v/v) rigid matrix at 77 K (all the compounds). The free ligands exhibit luminescence under all the experimental conditions used, while among the metal complexes only **2a** is luminescent, both at room temperature and at 77 K. Data are collected in Table 5, while some luminescence spectra are shown in Figure 6.

Luminescence energies and lifetimes of **1a–c** suggest that the excited state from which emission takes place is the lowest lying singlet π–π* level. Actually, emission spectra look like the spectral image (in particular, at room temperature) of the lowest lying π–π* absorption band. The emission maxima gradually move to lower energy in the series **1a**, **1b**, **1c** (Table 5, Figure 6a), in agreement with the attribution. That the emissive state also has a CT character, as mentioned in the absorption spectra discussion, is supported by the solvent dependence of the emission band: for example, the room temperature emission maximum of **1a** moves from 432 nm in dichloromethane to 442 nm in methanol, so indicating that the excited state has a larger dipolar nature than the ground state. This partial CT character, which suggests mixing with close lying n–π* states, also accounts for the quite low emission quantum yields (lower than 10^{-4}, see Table 5), which would be surprisingly low if a pure π–π* fluorescence was considered. At 77 K the luminescence lifetimes of the free ligands increase substantially (Table 5, Figure 6a); the spectra become structured and weakly blue-shifted. Altogether, these changes would suggest a reduced contribution at 77 K of the CT character in the emissive levels.

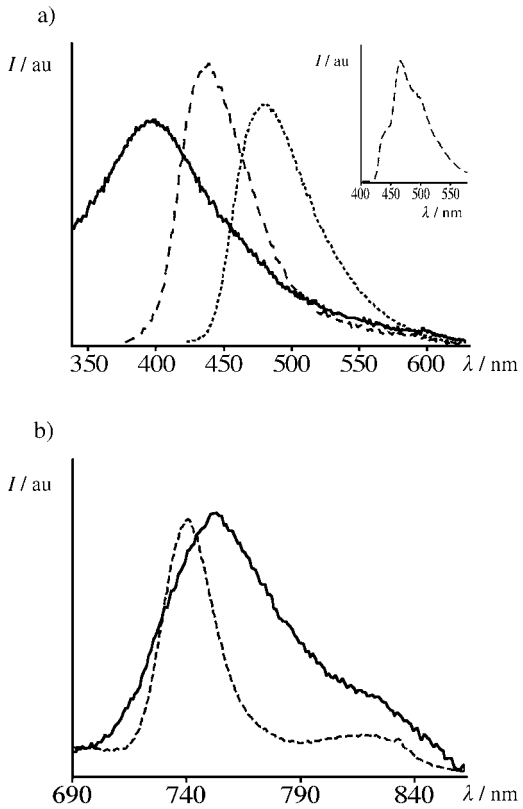

Figure 6. a) Luminescence spectra of **1a** (solid line), **1b** (dashed line) and **1c** (dotted line) in dichloromethane at room temperature and (inset) luminescence spectrum of **1b** in MeOH/EtOH 4:1 (v/v) at 77 K. b) Luminescence spectra of **2a** at room temperature in acetonitrile fluid solution (solid line) and at 77 K in an MeOH/EtOH 4:1 (v/v) rigid matrix (dashed line).

Ruthenium(II) polypyridine complexes are usually luminescent from their lowest lying ^{3}MLCT state.[14,22] However, complexes containing tridentate ligands (e.g., terpy), are scarcely luminescent at room temperature relative to species based on bidentate ligands (e.g., 2,2′-bipyridine).[14,22b] Recently, this drawback was overcome by several strategies, including the use of ligands having reduction potentials less negative.[2,23] The presence of such ligands moves the corresponding ^{3}MLCT state to low energies, so decreasing the efficiency of the activated process to the "poisoning" (with regard to the luminescence properties) ^{3}MC level. This approach anyway is sometimes a two-edged sword, since very low ^{3}MLCT states have diminished luminescence properties because the Franck–Condon factors for radiationless decay of the (potentially) luminescent level increase on decreasing the excited state energy (i.e., the basis of the so-called energy-gap law[24]). To obtain room-temperature emission from ruthenium(II) complexes, the above-mentioned effects have to be taken into account and suitably balanced. The rack-type complex **2a** indeed shows a relatively long-lived emission both at room temperature and at 77 K (Table 5, Figure 6b). The spectral shape, energy and lifetime, together with comparison with literature data,[14,22] indicate that such an emission can be straightforwardly attributed to the lowest-lying ^{3}MLCT state, in which the acceptor orbital is mainly centred on the substituted pyrimidine ring. The slight blue-shift of the emission spectrum and its longer lifetime on passing from room temperature fluid solution to 77 K rigid matrix are in line with the CT attribution.

The absence of emission within the wavelength region investigated ($\lambda < 850$ nm) for **2b** and **2c** is not surprising: in fact, on considering the energy of the singlet MLCT state as inferred by absorption spectroscopy (> 600 nm in both complexes), the corresponding triplet levels should lie at wavelength longer than 800 nm and could be out of the sensitivity range of our equipment (note that the band assigned in **2c** to the singlet–triplet absorption lies close to 800 nm, so the corresponding emission spectrum would be further displaced in the near-IR region). In these conditions, we cannot exclude that **2b** and **2c** can exhibit luminescence in the near-IR region, although it is expected that because of the energy-gap law, the eventual luminescence quantum yields would be extremely low.

Conclusion

New Ru^{II} bimetallic isomeric complexes (**2a**–**c**) with ditopic, isomeric hydrazone-based ligands were synthesized and characterized by several techniques, including NMR methods and crystallography. The absorption spectra, redox behaviour and luminescence properties of the new complexes and of the free ligands have been studied. The results indicate that the molecular diversity introduced by the isomerism translates into interesting differences as far as the spectroscopic, luminescence and redox properties of the ligands and the rack-type new metal complexes are concerned. For example, spin-allowed MLCT bands ($\lambda > 600$ nm) are present in **2b** and **2c**, while the lowest energy absorption MLCT band of **2a** lies at significantly higher energy. Moreover, while **2a** exhibits a typical ^{3}MLCT emission both in fluid solution at room temperature and in rigid matrix at 77 K, complexes **2b** and **2c** do not show any emission for $\lambda < 850$ nm. In general, it is shown that by taking advantage of relatively slight differences within the ditopic, isomeric hydrazone-based ligands strands, predetermined molecular architectures exhibiting significantly different properties can be obtained.

Preparation of tri- and poly-, homo- or heterometallic complexes of the same family, as well as their decoration with suitable groups able to modify their electronic properties in predetermined ways, could constitute further developments in this area of multicentre rack-type complexes. In particular, the combination of the specific redox properties with the difference in shape between the "lateral" complexes **2a** and **2b** and the "alternate" complex **2c** suggests the possibility to generate extended multicentre metallosupramolecular architectures of curved or linear, respectively, "metallomolecular wires".

Experimental Section

Materials and general methods: The following compounds were prepared as previously described: **1a**,**b**,[7] **3**,[11] **4**,[10] **5**,[10] **6**[9] and [Ru(terpy)Cl_3].[12] The following reagents were purchased from commercial sources: $RuCl_3$ (Aldrich, Avocado), terpy (Aldrich, Avocado), 2,5-dimethylpyrazine (Aldrich), benzaldehyde (Aldrich), benzoic anhydride (Aldrich). 400 MHz ^{1}H and 100 MHz ^{13}C NMR spectra were recorded on a Bruker Ultrashield Avance 400 spectrometer and 300 MHz ^{1}H and 75 MHz ^{13}C NMR spectra were recorded on a Bruker 300 spectrometer. The solvent residual signal[25] was used as an internal reference for both ^{1}H and ^{13}C NMR spectra. The following notation is used for the ^{1}H NMR spectral splitting patterns: singlet (s), doublet (d), triplet (t), multiplet (m). The 2D-NMR used experiments were: COSY (correlation spectroscopy), NOESY (Nuclear Overhauser enhancement spectroscopy or nuclear Overhauser and exchange spectroscopy), ROESY (rotating-frame Overhauser enhancement (effect) spectroscopy); they were done on 300 MHz or 500 MHz Bruker spectrometers. FAB-MS, EI-MS and ES-MS measurements were performed by the Service de Spectrométrie de Masse, Université Louis Pasteur. Melting points were recorded on a Büchi Melting Point B-540 apparatus and are uncorrected. UV/Vis spectra were recorded on a Varian-Cary-3 spectrometer or on a Jasco V-560 spectrometer. IR spectra were recorded on a Perkin–Elmer 1600-FTIR spectrometer; KBr pellets. Luminescence spectra were recorded on a Jobin-Yvon Spex Fluoromax P fluorimeter equipped with a Hamamatsu R3896 photomultiplier. Emission spectra have been corrected by the use of software purchased with the fluorimeter. Luminescence lifetimes were determined by time-correlated single-photon-counting (TCSPC) with an Edinburgh OB900 spectrometer (light pulse: Hamamatsu PL2 laser diode, pulse width 59 ps at 408 nm; or nitrogen discharge, pulse width: 2 ns). Electrochemical experiments were performed as previously described,[1f] with acetonitrile (metal complexes) or 1,2-dichloroethane (free ligands) as solvents. Experimental uncertainties are as follows: absorption maxima, 2 nm; emission maxima, 4 nm; emission lifetimes, 10%; redox potentials, 10 mV.

Crystal structure determinations: The crystals were obtained by diffusion–recrystallization by using pure acetonitrile (for **2c**) or a CH_3CN/CH_3OH 9:1 mixture (for **2a** and **2b**) as a solvent and Et_2O (for **2a** and **2b**) or iPr_2O (for **2c**) as a nonsolvent.

The crystals were placed in oil, and a single crystal was selected, mounted on a copper wire and placed in a low-temperature N_2 stream ($T=173$ K). The X-ray diffraction data were collected on a Nonius-Kappa-CCD diffractometer with graphite monochromatized $Mo_{K\alpha}$ radiation ($\lambda=0.71073$ Å), ϕ scans. The structures were solved by direct methods and refined (based on F^2 with all independent data) by full-matrix least-squares methods (OpenMolen package (for **2a** and **2c**) or SHELXL-97 (for **2b**)).

Data for 2a: Formula: $C_{105}H_{100}F_{48}N_{32}O_3P_8Ru_4$ ($2\,C_{48}H_{40}N_{14}Ru_2\cdot 8\,PF_6\cdot 4\,CH_3CN\cdot CH_3OH\cdot 2\,H_2O$); M_r: 3422.18; crystal system: triclinic; space group: $P\bar{1}$; cell dimensions: $a=14.5964(1)$, $b=20.5711(2)$, $c=25.0751(2)$ Å, $\alpha=102.860(5)°$, $\beta=105.329(5)°$, $\gamma=93.126(5)°$, $V=7027.5(1)$ Å^3; $Z=2$; colour: brown; crystal dimensions: $0.16\times0.13\times0.08$ mm; $\rho_{calcd}=1.62$ g cm^{-3}; $F(000)$: 3412; $\mu=0.635$ mm^{-1}; hkl limits: $-19,20/-28,28/-35,35$; θ range: $2.5\le\theta\le30.04°$; number of data measured: 61742; number of data with $I>3\sigma(I)$: 25682; number of variables: 1661; $R=0.085$; $R_w=0.114$; goodness-of-fit: 1.317; largest peak in final difference: 1.017 e Å^{-3}.

Data for 2b: Formula: $C_{54}H_{49}N_{17}Ru_2P_4F_{24}$ ($C_{48}H_{40}N_{14}Ru_2\cdot 4\,PF_6\cdot 3\,CH_3CN$); M_r: 1718.12; crystal system: monoclinic; space group: $P2_1/n$; cell dimensions: $a=14.882(5)$, $b=13.131(5)$, c = 34.498(5) Å, $\alpha=90.00(5)°$, $\beta=100.31(5)°$, $\gamma=90.00$ (5)°, V = 6633(4) Å^3; $Z=4$; colour: green; crystal dimensions: $0.10\times0.08\times0.05$ mm; $\rho_{calcd}=1.721$ g cm^{-3}; $F(000)$: 3424; $\mu=0.672$ mm^{-1}; hkl limits: $-20,20/0,18/0,48$; θ range: $1.20\le\theta\le30.05°$; number of data measured: 19356; number of data with $I>2\sigma(I)$: 10601; number of variables: 895; $R=0.0523$; $R_w=0.1682$; goodness-of-fit: 1.060.

Data for 2c: Formula: $C_{30}H_{29}F_{12}N_{10}P_2Ru$ (($C_{48}H_{40}N_{14}Ru_2\cdot 4\,PF_6\cdot 6\,CH_3CN$)/2); M_r: 920.63; crystal system: triclinic; space group: $P\bar{1}$; cell dimensions: $a=8.8208(2)$, $b=13.0232(3)$, $c=15.8342(4)$ Å, $\alpha=97.160(5)°$, $\beta=95.309(5)°$, $\gamma=90.199(5)°$, $V=1796.82(7)$ Å3; $Z=2$; colour: green; crystal dimensions: $0.20\times0.04\times0.02$ mm; $\rho_{calcd}=1.70$ g cm^{-3}; $F(000)$: 922; $\mu=0.627$ mm^{-1}; hkl limits: $-12,10/-18,18/-22,22$. θ range: $2.5\le\theta\le30.06°$; number of data measured: 16315; number of data with $I>3\sigma(I)$: 5635; number of variables: 496; $R=0.048$; $R_w=0.062$; goodness-of-fit: 1.059; largest peak in final difference: 1.286 e Å^{-3}.

CCDC-257649 (**2a**), CCDC-257650 (**2b**) and CCDC-257651 (**2c**) contain the supplementary crystallographic data for this paper. These data can be obtained free of charge from The Cambridge Crystallographic Data Centre via www.ccdc.cam.ac.uk/data_request/cif.

Pyrazine-2,5-dicarboxaldehydebis[methyl(pyridin-2-yl)hydrazone] (1c): A solution of hydrazine derivative **3** (100 mg, 0.813 mmol, 2.12 equiv) and dialdehyde **4** (52 mg, 0.382 mmol, 1 equiv) in EtOH (5 mL) was heated to reflux for 3 h. Then, the mixture was cooled and filtered. The precipitate was washed with EtOH and dried for 10 h under high vacuum: **1c** (86 mg, 65%). Yellow solid; m.p. 305°C; ^{1}H NMR (400 MHz, $CDCl_3$):$\delta=9.16$ (s, 2H; H_G), 8.26 (ddd, $J=1.0$, 2.0, 5.0 Hz, 2H; H_A), 7.76 (dt, $J=1$, 8.7 Hz, 2H; H_D), 7.74 (s, 2H; H_F), 7.66 (ddd, $J=2.0$, 7.0, 8.7 Hz, 2H; H_C), 6.87 (ddd, $J=1.0$, 5.0, 7.0 Hz, 2H; H_B), 3.73 ppm (s, 6H; H_E); ^{13}C NMR (75 MHz, $CDCl_3$): $\delta=157.26$, 148.63, 147.19, 140.89, 137.95, 132.29, 116.86, 110.41, 29.89 ppm; IR (KBr): $\tilde{\nu}=3004$ (w), 2902 (w), 1590 (s), 1560 (s), 1483 (s), 1435 (s), 1349 (s), 1213 (s), 1131 (s), 1029 (m), 921 (s), 868 (m), 770 (s), 731 (m), 613 cm^{-1} (w); UV/Vis ($CHCl_3$): $\lambda_{max}=247$, 409 nm; FAB-MS: m/z (%): 347.2 (100) $[M+H]^+$; HRMS (FAB-MS): calcd for $[C_{18}H_{18}N_8+H]^+$: 347.1733; found: 347.1737.

[{Ru(terpy)}$_2$(1a)](PF$_6$)$_4$ (2a): [Ru(terpy)Cl_3] (19.6 mg, 0.044 mmol, 2.2 equiv) and free ligand **1a** (7 mg, 0.020 mmol, 1equiv) were dissolved in ethanol/water (5 mL, 1:1 v/v). The mixture was heated under reflux for 19 h, then cooled to room temperature and filtered. Excess aqueous NH_4PF_6 was added to the solution and the precipitate was collected. The solid was purified by recrystallization from acetonitrile/Et_2O to afford **2a** (23 mg, 71%) as a brown solid. M.p. >300°C; ^{1}H NMR (400 MHz, CD_3CN): $\delta=8.93$ (s, 2H; H_E), 8.52 (d, $J=8.2$ Hz, 4H; H_M), 8.37 (t, $J=8.2$ Hz, 2H; H_N), 8.31 (d, $J=7.8$ Hz, 4H; H_L), 7.93–7.88 (m, 8H; H_K, H_I), 7.84 (d, $J=7.8$ Hz, 2H; H_D), 7.72–7.66 (m, 2H; H_C), 7.23–7.19 (m, 4H; H_J), 6.94–6.91 (m, 4H; H_A, H_B), 6.49 (s, 1H; H_G), 5.02 (s, 1H; H_H), 4.15 ppm (s, 6H; H_F); IR (KBr): $\tilde{\nu}=3110$ (w), 1614 (s), 1566 (w), 1527 (m), 1460 (s), 1391 (m), 1268 (m), 1122 (s), 1006 (w), 842 (s), 558 cm^{-1} (s); UV/Vis (CH_3CN): $\lambda_{max}=226$, 270, 308, 330, 362, 434, 470 nm; ES-MS: m/z calcd for $[Ru_2(\mathbf{1a})(terpy)_2(PF_6)_3]^+=[C_{48}H_{40}F_{18}N_{14}P_3Ru_2]^+$: 1451.1, found: 1451.1; calcd for $[Ru_2(\mathbf{1a})(terpy)_2(PF_6)_2]^{2+}=[C_{48}H_{40}F_{12}N_{14}P_2Ru_2]^{2+}$: 653.1, found: 652.8; calcd for $[Ru_2(\mathbf{1a})(terpy)_2PF_6]^{3+}=[C_{48}H_{40}F_6N_{14}PRu_2]^{3+}$: 387.0, found: 386.8; calcd for $[Ru_2(\mathbf{1a})(terpy)_2]^{4+}=[C_{48}H_{40}N_{14}Ru_2]^{4+}$: 254.1, found: 253.8.

[{Ru(terpy)}$_2$(1b)](PF$_6$)$_4$ (2b): [Ru(terpy)Cl_3] (19.6 mg, 0.044 mmol, 2.2 equiv) and free ligand **1b** (7 mg, 0.020 mmol, 1 equiv) were dissolved in ethanol/water (5 mL, 1:1 v/v). The mixture was heated under reflux for 20 h, then cooled to room temperature and filtered. Excess aqueous NH_4PF_6 was added to the solution and the precipitate was collected. The solid was purified by recrystallization from water, then from acetonitrile/Et_2O to afford **2b** (20 mg, 62%) as a green solid. M.p. >300°C; ^{1}H NMR (400 MHz, CD_3CN): $\delta=8.74$ (s, 2H; H_F), 8.56 (d, $J=8.1$ Hz, 4H; H_M), 8.43 (t, $J=8.1$ Hz, 2H; H_N), 8.32 (d, $J=8.1$ Hz, 4H; H_L), 7.90 (td, $J=1.6$, 8.1 Hz, 4H; H_K), 7.87 (d, $J=6.3$ Hz, 4H; H_I), 7.73 (s, 1H; H_G), 7.67 (ddd, $J=1.6$, 7.4, 8.8 Hz, 2H; H_C), 7.23–7.19 (m, 6H; H_D, H_J), 6.75 (dd, $J=1.0$, 5.5 Hz, 2H; H_A), 6.65 (ddd, $J=1.0$, 5.5, 7.4 Hz, 2H; H_B), 5.26 (s, 1H; H_H), 4.14 ppm (s, 6H; H_F); IR (KBr): $\tilde{\nu}=3111$ (w), 1603 (m), 1491 (m), 1436 (s), 1382 (w), 1321 (m), 1149 (m), 1109 (w), 838 (s), 767 (m), 558 cm^{-1} (s); UV/Vis (CH_3CN): $\lambda_{max}=240$, 270, 304, 330, 430, 506, 630 nm; ES-MS: m/z calcd for $[Ru_2(\mathbf{1b})(terpy)_2(PF_6)_3]^+=[C_{48}H_{40}F_{18}N_{14}P_3Ru_2]^+$: 1451.1, found: 1451.0; calcd for $[Ru_2(\mathbf{1b})(terpy)_2(PF_6)_2]^{2+}=[C_{48}H_{40}F_{12}N_{14}P_2Ru_2]^{2+}$: 653.1, found: 652.8; calcd for $[Ru_2(\mathbf{1b})(terpy)_2PF_6]^{3+}=[C_{48}H_{40}F_6N_{14}PRu_2]^{3+}$: 387.0, found: 386.8; calcd for $[Ru_2(\mathbf{1b})(terpy)_2]^{4+}=[C_{48}H_{40}N_{14}Ru_2]^{4+}$: 254.1, found: 253.8.

[{Ru(terpy)}$_2$(1c)](PF$_6$)$_4$ (2c): Ru(terpy)Cl_3 (19.6 mg, 0.044 mmol, 2.2 equiv) and free ligand **1c** (7 mg, 0.020 mmol, 1 equiv) were dissolved in ethanol/water (5 mL, 1:1 v/v). The mixture was heated under reflux for 20 h, then cooled to room temperature and filtered. Excess aqueous

NH_4PF_6 was added to the solution and the precipitate was collected. The solid was purified by recrystallization from acetonitrile/Et_2O to afford **2c** (19 mg, 59%) as a green solid. M.p. >300°C; ^{1}H NMR (400 MHz, CD_3CN): δ=8.73 (d, J=7.8 Hz, 4H; H_M), 8.52–8.46 (m, 6H; H_N, H_L), 8.28 (s, 2H; H_F), 7.98 (td, J=1.5, 7.8 Hz, 4H; H_K), 7.91 (d, J=5.9 Hz, 4H; H_I), 7.66 (ddd, J=1.0, 7.3, 8.8 Hz, 2H; H_C), 7.27 (ddd, J=1.0, 5.4, 6.9 Hz, 4H; H_J), 7.15 (d, J=8.8 Hz, 2H; H_D), 7.14 (s, 2H; H_G), 6.78 (dd, J=1.0, 6.0 Hz, 2H; H_A), 6.65–6.61 (m, 2H; H_B), 3.98 ppm (s, 6H; H_E); IR (KBr): $\tilde{\nu}$=3095 (w), 1605 (m), 1509 (s), 1468 (s), 1404 (s), 1317 (m), 1198 (m), 1036 (w), 837 (s), 766 (s), 557 cm^{-1} (s); UV/Vis (CH_3CN): λ_{max}=272, 280, 304, 440, 614, 772 nm; ES-MS: m/z calcd for $[Ru_2(\mathbf{1c})(terpy)_2(PF_6)_3]^+$=$[C_{48}H_{40}F_{18}N_{14}P_3Ru_2]^+$: 1451.1, found: 1451.0.

2,5-Pyrazinedicarboxaldehyde (4): Compound **4** was prepared by ozonolysis of **6**, as previously described.[10] It was purified by recrystallization (reprecipitation) from a $CHCl_3$/$i$$Pr_2O$ mixture. Yield 20–30%; yellowish solid; m.p. 124–125°C; ^{1}H NMR (400 MHz, $CDCl_3$): δ=10.23 (s, 2H), 9.30 ppm (s, 2H); ^{13}C NMR (100 MHz, $CDCl_3$): δ=191.79, 148.77, 143.41 ppm; UV/Vis ($CHCl_3$): λ_{max}=280 nm; EI-MS: m/z (%): 136.1 (100) $[M]^+$, 107.1 (47) $[M-29]^+$, 80.0 (12) $[M-56]^+$, 52.1 (34) $[M-84]^+$, 29.1 (11) $[M-107]^+$; HRMS (EI-MS): calcd for $[C_6H_4O_2N_2]^+$:136.0273; found: 136.0275.

2,5-(*E*,*E*)-Distyrylpyrazine (6): Compound **6** was prepared by condensation of benzaldehyde with 2,5-dimethylpyrazine, as previously described.[9] Yellow solid; m. p. 224°C; ^{1}H NMR (300 MHz, $CDCl_3$): δ= 8.60 (s, 2H), 7.74 (d, J=16.1 Hz, 2H), 7.61 (d, J=7.2 Hz, 4H), 7.44–7.30 (m, 6H), 7.18 ppm (d, J=16.1 Hz, 2H); ^{13}C NMR (75 MHz, $CDCl_3$): δ= 149.24, 143.42, 136.42, 134.53, 128.99, 127.44, 124.25 ppm (two overlaping peaks); UV/Vis ($CHCl_3$): λ_{max}=305, 384 nm.

Acknowledgements

We thank Dr. Annie Marquis and Raymond Hueber for mass spectrometry analyses. A.-M.S. thanks le Ministère de la Recherche, de la Jeunesse et de la Technologie for a predoctoral fellowship. S.C. also acknowledges MIUR and FIRB for financial support.

[1] a) G. S. Hanan, C. Arana, J.-M. Lehn, D. Fenske, *Angew. Chem.* **1995**, *107*, 1191; *Angew. Chem. Int. Ed. Engl.* **1995**, *34*, 1122; b) G. S. Hanan, C. Arana, J.-M. Lehn, G. Baum, D. Fenske, *Chem. Eur. J.* **1996**, *2*, 1292; c) B. Hasenknopf, J. Hall, J.-M. Lehn, V. Balzani, A. Credi, S. Campagna, *New J. Chem.* **1996**, *20*, 725; d) P. Ceroni, A. Credi, V. Balzani, S. Campagna, G. S. Hanan, C. Arana, J.-M. Lehn, *Eur. J. Inorg. Chem.* **1999**, *9*, 1409; e) M. Ruben, E. Breuning, M. Barboiu, J.-P. Gisselbrecht, J.-M. Lehn, *Chem. Eur. J.* **2003**, *9*, 291; f) D. M. Bassani, J, -M. Lehn, S. Serroni, F. Puntoriero, S. Campagna, *Chem. Eur. J.* **2003**, *9*, 5936.

[2] a) M. Maestri, N. Armaroli, V. Balzani, E. C. Constable, A. M. W. Cargill Thompson, *Inorg. Chem.* **1995**, *34*, 2759; b) J.-P. Sauvage, J. P. Collin, J. C. Chambron, S. Guillerez, C. Coudret, V. Balzani, F. Barigelletti, L. De Cola, L. Flamigni, *Chem. Rev.* **1994**, *94*, 993; c) A. Elghayoury, A. Harriman, A. Khatyr, R. Ziessel, *Angew. Chem.* **2000**, *112*, 191; *Angew. Chem. Int. Ed.* **2000**, *39*, 185; d) A. El-ghayoury, A. Harriman, A. Khatyr, R. Ziessel, *J. Phys. Chem. A* **2000**, *104*, 1512; e) F. Barigelletti, L. Flamigni, *Chem. Soc. Rev.* **2000**, *29*, 1; f) F. Loiseau, R. Passalacqua, S. Campagna, M. I. J. Polson, Y.-Q. Fang, G. S. Hanan, *Photochem. Photobiol. Sci.* **2002**, *1*, 982; g) S. Encinas, L. Flamigni, F. Barigelletti, E. C. Constable, C. E. Housecroft, E. R. Schofield, E. Figgemeier, D. Fenske, M. Neuburger, J. G. Vos, M. Zehnder, *Chem. Eur. J.* **2002**, *8*, 137.

[3] M. Benaglia, F. Ponzini, C. R. Woods, J. S. Siegel, *Org. Lett.* **2001**, *3*, 967.

[4] D. Brown, S. Murajan, Y. Jang, R. Thummel, *Org. Lett.* **2002**, *4*, 1253.

[5] J.-M. Lehn, *Supramolecular Chemistry: Concepts and Perspectives*, VCH, Weinheim, **1995**.

[6] K. M. Gardinier, R. G. Khoury, J.-M. Lehn, *Chem. Eur. J.* **2000**, *6*, 4124.

[7] J.-L. Schmitt, A.-M. Stadler, N. Kyritsakas and J.-M. Lehn, *Helv. Chim. Acta* **2003**, *86*, 1598.

[8] a) T. Bark, M. Düggeli, H. Stoeckli-Evans, A. von Zelewsky, *Angew. Chem.* **2001**, *113*, 2924; *Angew. Chem. Int. Ed.* **2001**, *40*, 2848; b) T. Bark, H. Stoeckli-Evans, A. von Zelewsky, *J. Chem. Soc. Perkin Trans. 1*, **2002**, 1881.

[9] R. Franke, *Ber. Dtsch. Chem. Ges.* **1905**, *38*, 3724.

[10] a) R. H. Wiley, U. S. Pat. 4, 260,757, **1981**; b) R. H. Wiley, *J. Macromol. Sci. Chem.* **1987**, *A24*, 1183.

[11] M. A. Baldo, G. Chessa, G. Marangoni, B. Pitteri, *Synthesis* **1987**, 720.

[12] B. P. Sullivan, J. M. Calvert, T. J. Meyer, *Inorg. Chem.* **1980**, *19*, 1404.

[13] A.-M. Stadler, J.-M. Lehn, unpublished results.

[14] A. Juris, V. Balzani, F. Barigelletti, S. Campagna, P. Belser, A. von Zelewsky, *Coord. Chem. Rev.* **1988**, *84*, 85, and references therein.

[15] a) J. E. Sutton, H. Taube, *Inorg. Chem.* **1981**, *20*, 3125; b) C. Creutz, *Prog. Inorg. Chem.* **1983**, *30*, 1; c) N. S. Hush, *Coord. Chem. Rev.* **1985**, *64*, 135; d) S. Ernst, V. Kasack, W. Kaim, *Inorg. Chem.* **1988**, *27*, 1146; e) G. Giuffrida, S. Campagna, *Coord. Chem. Rev.* **1994**, *135*, 517; f) M. D. Ward, *Chem. Soc. Rev.* **1995**, *24*, 121; g) B. D. Yeomans, L. S. Kelso, P. A. Tregloan, F. R. Keene, *Eur. J. Inorg. Chem.* **2001**, 239.

[16] a) A. A. Vlceck, *Coord. Chem. Rev.* **1982**, *43*, 39; b) M. Marcaccio, F. Paolucci, C. Paradisi, S. Roffia, C. Fontanesi, L. J. Yellowlees, S. Serroni, S. Campagna, G. Denti, V. Balzani, *J. Am. Chem. Soc.* **1999**, *121*, 10081, and references therein.

[17] It should be considered that redox data refers to solution, while X-ray determination indicates "frozen" solid-state situations. However it appears reasonable that in the average, distance differences can also exist in solution.

[18] H. H. Jaffé, M. Orchin, *Theory and Applications of Ultraviolet Spectroscopy*, Wiley, **1964**, Chapter 14.

[19] M. Klessinger, J. Michl, *Excited States and Photochemistry of Organic Molecules*, VCH, New York, **1995**.

[20] A. Giannetto, G. Guglielmo, V. Ricevuto, A. Giuffrida, S. Campagna, *J. Photochem. Photobiol. A* **1990**, *53*, 23.

[21] J. Andersson, F. Puntoriero, S. Serroni, A. Yartsev, T. Pascher, T. Polivka, S. Campagna, V. Sundström, *Chem. Phys. Lett.* **2004**, *386*, 336.

[22] a) G. R. Crosby, *Acc. Chem. Res.* **1975**, *8*, 231; b) T. J. Meyer, *Pure Appl. Chem.* **1986**, *58*, 1193.

[23] M. I. J. Polson, E. A. Medlycott, G. S. Hanan, L. Mikelsons, N. J. Taylor, M. Watanabe, Y. Tanaka, F. Loiseau, R. Passalacqua, S. Campagna, *Chem. Eur. J.* **2004**, *10*, 3640.

[24] a) W. Siebrand, *J. Chem. Phys.* **1967**, *46*, 440; b) J. V. Caspar, T. J. Meyer, *J. Phys. Chem.* **1983**, *87*, 952.

[25] H. E. Gottlieb, V. Kotlyar, A. Nudelman, *J. Org. Chem.* **1997**, *62*, 7512.

Received: December 8, 2004
Published online: April 21, 2005

